

# High-power handling and bias stability of thin-film Lithium Tantalate microring and coupling resonators

Ayed Al Sayem, Shiekh Zia Uddin, Ting-Chen Hu, Alaric Tate, Mark Cappuzzo, Rose Kopf, Mark Earnshaw  
*Nokia Bell Labs, Murray Hill, NJ, USA*  
(Dated: February 3, 2026)

In this paper, we demonstrate the ultra-high-power handling capability and DC bias stability of optical microring and electro-optic (EO) coupling resonators on the thin-film lithium tantalate (TFLT) platform. We show that, with annealing, oxide cladded TFLT resonators can handle several watts ( $\sim 4$  W) of circulating power with minimal frequency shift and no observable photo-refractive effect. Furthermore, we demonstrate a compact 2 mm coupling modulator achieving a low  $V_\pi$  of 3 V with stable bias and phase control in the telecom C-band.

## INTRODUCTION

Thin-film lithium niobate (TFLN) has been developed over the past decade and is currently one of the primary candidate platforms for next-generation optical communication networks for both short-haul and long-haul communications [1]. TFLN fabrication is now mature. However, LN suffers strongly from the photo-refractive (PR) effect, which severely limits the power handling capability and makes devices unstable, limiting practical applications. The PR effect is challenge to wide adoption of TFLN devices for numerous applications, due to the need to limit the optical power and the hindrance to stable operation [2–5]. Although ultra-efficient photonic devices on the TFLN platform have been demonstrated, such as ultra-low threshold parametric oscillator [4], photon-pair generation [6], microwave to optical quantum transducer [3, 7, 8], low-drive ultra high speed modulator [9], instability, and drift due to the PR effect fundamentally limits device performance [2, 10]. Normalized efficiency is exceptionally high for many of the demonstrations on the TFLN platform, but the inability to increase on-chip optical power directly hinders practical applications. The PR effect also causes DC bias instability [11, 12], which makes stable low-power bias circuits not possible on TFLN [11]. The thermo-optic (TO) effect can be used for bias control for traveling wave-modulator [11], or resonators [13]. However, as the TO effect is weak for the LN platform, it causes very high static power consumption [11]. This then prevents scaling to practical, large-scale, photonic circuits on TFLN, where many such bias circuits are necessary. Especially for quantum applications where cryogenic stable bias circuits are required [14], TFLN loses its fundamental advantage of the EO effect due to this instability [3, 7, 8].

Lithium tantalate (LT) has very similar electro-optic (EO) properties but offers much higher optical damage threshold than LN [15–18]. Some early demonstrations have shown very promising results on the TFLT platform such as low propagation loss [19], high-rate data modulation [20, 21], frequency comb generation

[22] etc. The open question is whether TFLT can perform with similar efficiency as TFLN but with proper stable operation, which can pave the way from proof-of-principle demonstrations to real-world applications. In this article, we study the dynamics of optical micro-ring resonators on the TFLT platform at very high optical power (up to 4 W) and show that even with such high circulating power, the TO effect is dominant over the PR effect. With annealing, we cannot distinguish any observable PR effect. We show that TFLT has orders of magnitude better optical power handling than TFLN, AlGaAs, and  $Ta_2O_5$  but slightly worse than SiN. For a complete picture, we also study the stability of a coupling modulator on the TFLT platform which is a direct application for high-speed optical communications [9, 23]. This is the first demonstration of a coupling modulator on the TFLT platform and we show exceptional enhanced modulation efficiency of just 3 V  $V_\pi$  with only 2 mm long modulation section ( $0.6 \text{ Vcm } V_\pi L$ ). We show stable bias and phase control of the coupling modulator, thereby enabling practical utilization for ultra-high speed and low energy optical communication with stable resonant EO modulators.

## PR EFFECT ON TFLT MICRORING RESONATOR

Fig.1(a) shows the optical image of the micro-ring resonator used in this paper. The cross-section of the micro-ring resonator in the coupling section is shown in the inset of Fig.1(a). The device fabrication starts with a 4-inch TFLN wafer on a silicon substrate commercially available from NanoLN. Photonic devices are photo-lithographically defined and subsequently etched using  $Ar^+$  plasma. After etching the optical device layer,  $1.5 \mu\text{m}$  thick oxide is deposited using plasma-enhanced chemical vapor deposition (PECVD). Co-planar waveguide electrode layers are defined by photolithography and subsequent etching or lift-off process for the coupling resonator. The wafer was diced, and the individual chips were polished for efficient fiber-

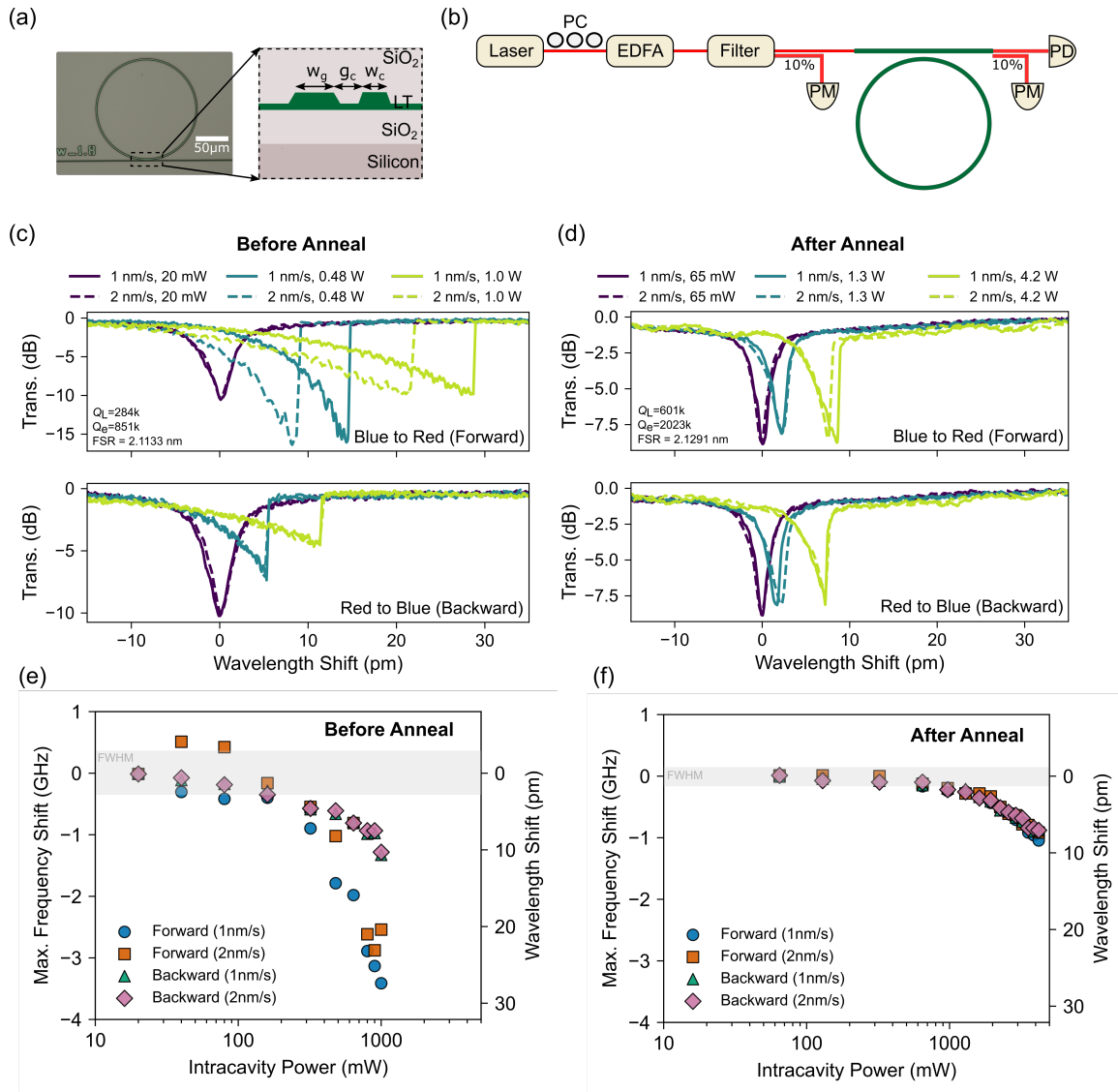


**FIG. 1. Device architecture and high-power characterization of the TFLN micro-ring resonator:** (a) Optical microscope image of the fabricated thin-film lithium niobate (TFLN) micro-ring resonator (50  $\mu\text{m}$  scale bar). The inset shows a cross-sectional schematic of the coupling section, highlighting the etched rib waveguide structure on a silicon substrate. (b) Schematic of the high-power measurement setup, incorporating an Erbium-Doped Fiber Amplifier (EDFA) and a tunable filter to characterize the resonator's nonlinear response. (c-d) Power-dependent transmission spectra before (c) and after (d) thermal annealing. The spectra compare forward (blue-to-red) and backward (red-to-blue) wavelength scans at various speeds (1 nm/s and 2 nm/s). Post-annealing results show significantly reduced resonance distortion and thermal bistability. (e-f) Extracted maximum resonance frequency shift as a function of intracavity power before (e) and after (f) annealing. The annealed device demonstrates superior power handling, with resonance shifts remaining within the Full-Width at Half-Maximum (FWHM) for intracavity powers up to approximately 1 W.

to-chip coupling.

Fig.1(b) shows the measurement setup. Light from a tunable laser (Santec-570) is first amplified by an erbium-doped fiber amplifier (EDFA) and filtered by a bandpass filter with a bandwidth of 10 nm. Output light from the filter is then coupled to the DUT using a lensed fiber. A fiber-based splitter is used before the DUT to monitor the launched optical power in a slow optical power meter (PM). A polarization controller (PC) is used to optimize

the polarization for the TE mode. After passing through the device, the light is coupled to another lens fiber. A second fiber splitter is used to monitor the output power from the device using another optical PM. The other output of the fiber splitter is sent to a fast photo-detector (PD).

We first measure the as-fabricated microring resonators with PECVD oxide cladding and without any annealing. Oxide cladding is necessary for proper

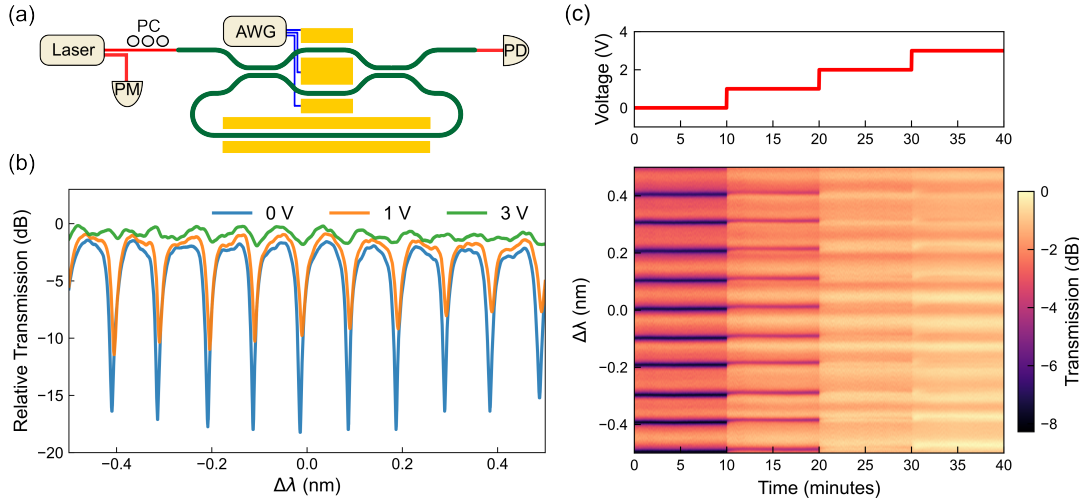


FIG. 2. **Characterization of the coupling modulator:** (a) Schematic of the experimental setup for characterizing the device, including a laser source, polarization controller (PC), and power meter (PM). The arbitrary waveform generator (AWG) provides voltage to the Signal (S) and Ground (G) electrodes of the coupling modulator, which has an active length of 2 mm. (b) Relative transmission spectra at bias voltages of 0 V, 1 V, and 3 V. (c) Top: Applied DC bias voltage stepped from 0 V to 3 V in 1 V increments every 10 minutes. Bottom: Time-resolved transmission heatmap showing the spectral response over a 40-minute duration.

velocity matching to achieve high-speed modulation [24], hence we study the optical power handling only with oxide cladding. In Fig.1(c), we plot the transmission from the device as a function of wavelength. Here, we scan in both forward (blue to red) and backward (red to blue) directions with different scan speeds. Material platforms such as LN or LT, which have a PR effect, can show distinctive behavior with respect to scan direction as the PR effect blue shifts the resonance, whereas the thermo-optic (TO) effect red shifts the resonance [2]. With forward scanning, the strong PR effect also reduces the linewidth of the resonance, making the fitted quality factor,  $Q_L$ , artificially high. Such effects have been observed to be quite drastic for TFLN [2]. As can be observed from Fig.1(c), forward and backward scans show different dynamics. With forward scanning, we observe a larger frequency shift than with backward scanning. This TFLT behavior is the opposite to that of TFLN [2] and confirms the PR effect is weaker than the TO effect in TFLT. In Fig.1(e), we show the maximum frequency shift as a function of intra-cavity power before annealing. With 1 W of intra-cavity power, we observe a maximum frequency shift of  $\sim 3.5$  GHz. We then anneal the device at  $500^\circ\text{C}$  for 2 hours and redo the measurement. After annealing, we observe a negligible difference in the resonance shape and a similar frequency shift for both forward and backward scanning, which can be observed from Fig.1(d). The quality factor of the devices also increases by a factor of  $\sim 2$  after annealing. In Fig.1(f), we show the maximum frequency shift as a function of intra-cavity power after annealing. The frequency shift decreases from  $\sim 3.5$  GHz to  $\sim 160$  MHz

at 1 W of intra-cavity power. With  $\sim 4$  W of intra-cavity power, we only observe  $\sim 1$  GHz frequency shift. There is also only a small difference in the frequency shift for forward and backward scanning at any power level, indicating minimal PR effect. We compare the rate of normalized TO-induced frequency shift as a function of energy density of a microring resonator for different material platforms in Table I. Similar to Ref. [25], we use energy density as it is independent of the device geometry and quality factors which vary for different material platforms. From Table I, we see that the TFLT platform performs better than TFLN by  $\sim 9$  order of magnitude. Only SiN performs better in terms of TO frequency shift than TFLT. The details of the theoretical calculation of the resonance frequency shift including photo-refractive and photo-thermal effect is provided in the supplementary information.

TABLE I. Photo-thermal Stability Comparison

Material	Stability Factor* (mJ <sup>-1</sup> cm <sup>3</sup> )	Ref.
Si <sub>3</sub> N <sub>4</sub>	$2.6 \times 10^{-8}$	[25]
Si	$1.0 \times 10^{-4}$	[26]
Ta <sub>2</sub> O <sub>5</sub>	$8.8 \times 10^{-7}$	[25]
Al <sub>0.2</sub> Ga <sub>0.8</sub> As	$2.1 \times 10^{-6}$	[25]
TFLN (Oxide Coated)	$4.2 \times 10^2$	[2]
<b>TFLT (Before Anneal)</b>	$9.5 \times 10^{-7}$	<b>This Work</b>
<b>TFLT (After Anneal)</b>	$1.8 \times 10^{-7}$	<b>This Work</b>

\*Defined as  $\frac{1}{\omega_0} \frac{\partial \delta\omega_m}{\partial \rho}$ , where  $\delta\omega_m$  is the resonance frequency shift,  $\rho$  is the intracavity energy density, and  $\omega_0$  is the resonance frequency.

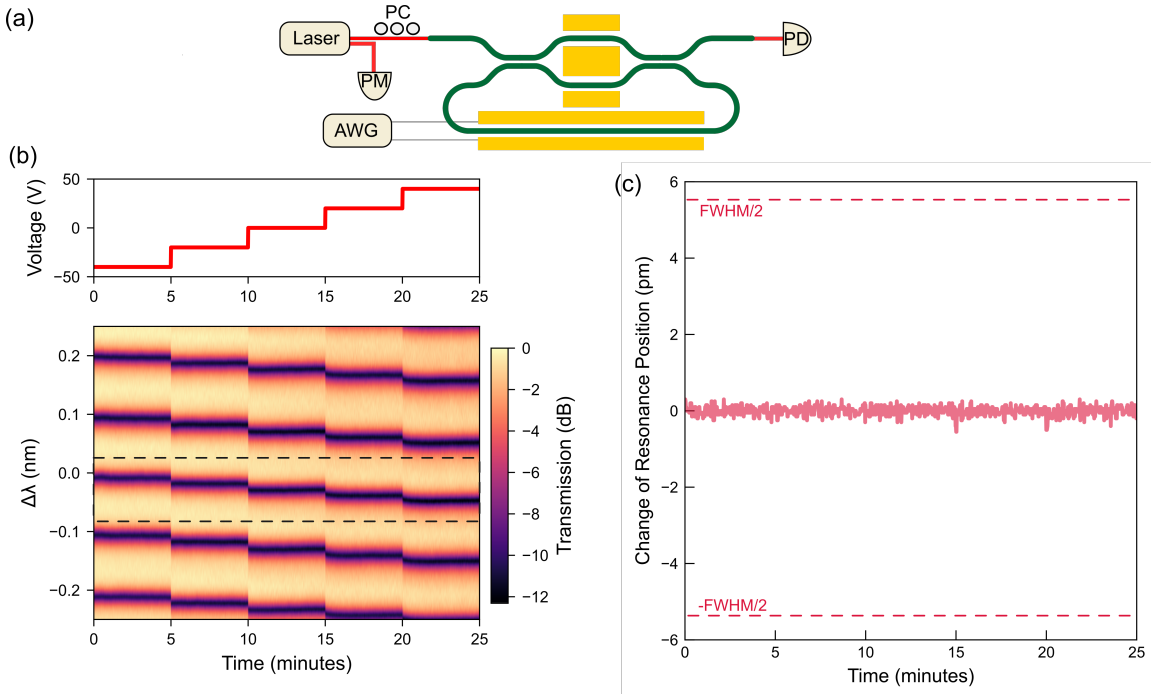


**FIG. 3. Phase stability and repeatability:** (a) Schematic of the experimental setup used for phase stability measurements, featuring a laser source, polarization controller (PC), power meter (PM), and an arbitrary waveform generator (AWG) to drive the electrodes, with the output captured by a photodetector (PD). (b) Top: Applied phase bias voltage applied in discrete steps. Bottom: Corresponding transmission spectra over time, showing the resonance shift as a function of the stepped voltage. (c) Stability analysis showing the change in resonance position over 25 minutes. The resonance shift remains below 0.1 pm, well within the half-maximum (FWHM) boundaries.

### BIAS STABILITY OF COUPLING MODULATORS

Conventional traveling wave electro-optic modulators on the TFLN and TFLT platforms are primarily limited in drive voltage and RO bandwidth [24, 27] by RF loss from the electrodes [20, 24]. Ring modulators where the ring resonant wavelength is tuned have been shown to enhance modulation efficiency but are limited by photon lifetime. Coupling modulators modulate the resonator coupling strength so the photon-lifetime is directly modulated. Thus, the EO bandwidth of such a modulator is no longer limited by the photon-lifetime [9, 23]. Coupling modulators can thus break the voltage-bandwidth constraint and have been demonstrated on the TFLN platform [9, 13]. Although coupling modulators have been demonstrated on the TFLN platform [9, 13], the large PR effect [2, 5] prevents use in practical applications where high power (eg: 10-100mW used in modern communication) and, most importantly, stable operation is necessary. Here, we show a coupling resonator/modulator on the TFLT platform for the first time and study the bias and phase stability of the EO modulation as a function of time. Fig.2 shows the measurement setup for the coupling modulator. Light from a fast scanning laser (Santec-570) is coupled to

the DUT using a lens fiber. A polarization controller is used to launch TE mode only. An arbitrary waveform generator (AWG) is used to drive the modulator at different bias voltages. The length of the modulator electrodes is  $L_{MZI} = 2$  mm. The details of the coupling modulator design and system-level measurement results will be presented in a separate work. In this paper, we focus on the bias stability. Fig.2(b) shows the transmission from the device as a function of wavelength when different bias voltages are applied. At  $V_{bias} = 0$  V, the resonator is critically coupled, showing a dip in the transmission. At  $V_{bias} = 3$  V, the coupling condition changes from a critical coupled to extremely uncoupled (no-coupling) with an extinction of more than 15 dB and with minimal frequency shift. The equivalent  $V_{pi}$  of a straight waveguide modulator is 14 V, hence the  $V_{pi}$  is  $\sim 4.7$  times improved. Further enhancement can be achieved with a higher optical quality factor, which can be achieved either through annealing or with a more effective dry and wet etching recipe. In Fig.2(c), we plot the transmission of the coupling modulator as a function of time for different bias voltages. We observe no major shift in transmission at different bias voltages, indicating ultra-stable operation. In Fig.3(b) and Fig.3(c), we show the phase repeatability of the resonator itself as a function of the resonator bias instead of the coupling

bias as shown in Fig.3(a). We apply a high voltage to the resonator arm, ranging from  $-50$  V to  $50$  V, and measure the transmission from the device as a function of time. We observe negligible transmission drift as a function of time, even with high DC voltages, as can be observed from Fig.3(b) and Fig.3(c).

## CONCLUSION

In conclusion, we demonstrate that with proper annealing, oxide-cladded photonic devices such as micro-ring resonators on the TFLT platform can handle watt-level power with minimal degradation due to the PR effect. We also demonstrate the first coupling modulator on the TFLT platform with stable bias and a V<sub>pi</sub> of just  $3$  V with a short  $2$  mm modulation electrode. These findings will pave the way for many practical classical and quantum devices on the TFLT platform.

## FUNDING

Nokia Corporation of America.

- 
- [1] Di Zhu, Linbo Shao, Mengjie Yu, Rebecca Cheng, Boris Desiatov, CJ Xin, Yaowen Hu, Jeffrey Holzgrafe, Soumya Ghosh, Amirhassan Shams-Ansari, et al. Integrated photonics on thin-film lithium niobate. *Advances in Optics and Photonics*, 13(2):242–352, 2021.
- [2] Yuntao Xu, Mohan Shen, Juanjuan Lu, Joshua B Surya, Ayed Al Sayem, and Hong X Tang. Mitigating photorefractive effect in thin-film lithium niobate microring resonators. *Optics Express*, 29(4):5497–5504, 2021.
- [3] Yuntao Xu, Ayed Al Sayem, Linran Fan, Changling Zou, and Hong X Tang. Bidirectional electro-optic conversion reaching 1% efficiency with thin film lithium niobate. In *CLEO: Science and Innovations*, pages SM4L–4. Optica Publishing Group, 2021.
- [4] Juanjuan Lu, Ayed Al Sayem, Zheng Gong, Joshua B Surya, Chang-Ling Zou, and Hong X Tang. Ultralow-threshold thin-film lithium niobate optical parametric oscillator. *Optica*, 8(4):539–544, 2021.
- [5] Xuan Sun, Hanxiao Liang, Rui Luo, Wei C Jiang, Xi-Cheng Zhang, and Qiang Lin. Nonlinear optical oscillation dynamics in high-q lithium niobate microresonators. *Optics Express*, 25(12):13504–13516, 2017.
- [6] Zhaohui Ma, Jia-Yang Chen, Zhan Li, Chao Tang, Yong Meng Sua, Heng Fan, and Yu-Ping Huang. Ultrabright quantum photon sources on chip. *Physical Review Letters*, 125(26):263602, 2020.
- [7] Timothy P. McKenna, Jeremy D. Witmer, Rishi N. Patel, Wentao Jiang, Raphaël Van Laer, Patricio Arrangoiz-Arriola, E. Alex Wollack, Jason F. Herrmann, and Amir H. Safavi-Naeini. Cryogenic microwave-to-optical conversion using a triply-resonant lithium-niobate-on-sapphire transducer. *Optica*, 7(12):1737–1744, 2020.
- [8] Jeffrey Holzgrafe, Neil Sinclair, Di Zhu, Amirhassan Shams-Ansari, Marco Colangelo, Yaowen Hu, Mian Zhang, Karl K. Berggren, and Marko Lončar. Cavity electro-optics in thin-film lithium niobate for efficient microwave-to-optical transduction. *Optica*, 7(12):1714–1720, 2020.
- [9] Yu Xue, Ranfeng Gan, Kaixuan Chen, Gengxin Chen, Ziliang Ruan, Junwei Zhang, Jie Liu, Daoxin Dai, Changjian Guo, and Liu Liu. Breaking the bandwidth limit of a high-quality-factor ring modulator based on thin-film lithium niobate. *Optica*, 9(10):1131–1137, 2022.
- [10] Tummas Napoleon Arge, Seongmin Jo, Huy Quang Nguyen, Francesco Lenzini, Emma Lomonte, Jens Arnbak Holbøll Nielsen, Renato R. Domeneguetti, Jonas Schou Neergaard-Nielsen, Wolfram Pernice, Tobias Gehring, and Ulrik Lund Andersen. Demonstration of a squeezed light source on thin-film lithium niobate with modal phase matching. *Optica Quantum*, 3(5):467–473, 2025.
- [11] Mengyue Xu, Mingbo He, Hongguang Zhang, Jian Jian, Ying Pan, Xiaoyue Liu, Lifeng Chen, Xiangyu Meng, Hui Chen, Zhaohui Li, et al. High-performance coherent optical modulators based on thin-film lithium niobate platform. *Nature communications*, 11(1):3911, 2020.
- [12] Hana K. Warner, Yuqi Zhao, Yu Zhang, Mian Zhang, and Marko Lončar. Dc-stable thin-film lithium niobate modulator at liquid nitrogen temperatures. *Optics Letters*, 50(17):5398–5401, 2025.
- [13] Ayed Al Sayem, Heqing Huang, Ting-Chen Hu, Mark Cappuzzo, Alaric Tate, Rose Kopf, and Mark Earnshaw. Multi-stage racetrack mach zehnder coupling interferometer on tfln with thermal and electro-optic modulation. In *CLEO: Applications and Technology*, page AA124.8. Optica Publishing Group, 2025.
- [14] A manufacturable platform for photonic quantum computing. *Nature*, 641(8064):876–883, 2025.
- [15] Xiaolong Yan, Yao Liu, Liang Ge, et al. High optical damage threshold on-chip lithium tantalate microdisk resonator. *Optics Letters*, 45(15):4100–4103, 2020.
- [16] F. Holtmann, J. Imbrock, C. B”aumer, et al. Photorefractive properties of undoped lithium tantalate crystals for various compositions. *Journal of Applied Physics*, 96(12):7455–7459, 2004.
- [17] O. Althoff and E. E. Kr”atzig. Strong light-induced refractive index changes in linbo3. In P. Guenter, editor, *Nonlinear Optical Materials III*, volume 1273, pages 12–19. SPIE, 1990.
- [18] Y. Kong, F. Bo, W. Wang, et al. Recent progress in lithium niobate: Optical damage, defect simulation, and on-chip devices. *Advanced Materials*, 32(3):1806452, 2020.
- [19] Chengli Wang, Zihan Li, Johann Riemensberger, Grigory Lihachev, Mikhail Churaev, Wil Kao, Xinru Ji, Junyin Zhang, Terence Blesin, Alisa Davydova, et al. Lithium tantalate photonic integrated circuits for volume manufacturing. *Nature*, 629(8013):784–790, 2024.
- [20] Chengli Wang, Dengyang Fang, Junyin Zhang, Alexander Kotz, Grigory Lihachev, Mikhail Churaev, Zihan Li, Adrian Schwarzenberger, Xin Ou, Christian Koos, et al. Ultrabroadband thin-film lithium tantalate modulator for high-speed communications. *Optica*, 11(12):1614–1620, 2024.

- [21] Margot Niels, Tom Vanackere, Ewoud Vissers, Tingting Zhai, Patrick Nenezic, Jakob Declercq, Cédric Bruynsteen, Shengpu Niu, Arno Moerman, Olivier Caytan, et al. A high-speed heterogeneous lithium tantalate silicon photonics platform. *arXiv preprint arXiv:2503.10557*, 2025.
- [22] Junyin Zhang, Chengli Wang, Connor Denney, Johann Riemensberger, Grigory Lihachev, Jianqi Hu, Wil Kao, Terence Blésin, Nikolai Kuznetsov, Zihan Li, et al. Ultrabroadband integrated electro-optic frequency comb in lithium tantalate. *Nature*, 637(8048):1096–1103, 2025.
- [23] X. Chen, A. Mistry, M. Bahaduri, K. Padmaraju, M. Malinowski, D. Che, R. Sukkar, R. Younce, A. Horth, Y. Dziashko, D. Gill, A. Seyoum, J. Naik, D. Lim, A. El Sayed, A. Rylyakov, M. Schmidt, Z. Luo, R. Patel, P. Magill, G. Burrell, J. Basak, D. Chapman, A. Mikami, Y. Man, M. Astolfi, A. Leven, and N. A. F. Jaeger. Free-spectral-range-free microring-based coupling modulator with integrated contra-directional couplers. *Journal of Lightwave Technology*, 42(12):4296–4301, 2024. Published online ahead of print.
- [24] Mian Zhang, Cheng Wang, Prashanta Kharel, Di Zhu, and Marko Lončar. Integrated lithium niobate electro-optic modulators: when performance meets scalability. *Optica*, 8(5):652–667, 2021.
- [25] Maodong Gao, Qi-Fan Yang, Qing-Xin Ji, Heming Wang, Lue Wu, Boqiang Shen, Junqiu Liu, Guanhao Huang, Lin Chang, Weiqiang Xie, et al. Probing material absorption and optical nonlinearity of integrated photonic materials. *Nature Communications*, 13(1):3323, 2022.
- [26] Marc De Cea, Amir H Atabaki, and Rajeev J Ram. Power handling of silicon microring modulators. *Optics express*, 27(17):24274–24285, 2019.
- [27] Prashanta Kharel, Christian Reimer, Kevin Luke, Lingyan He, and Mian Zhang. Breaking voltage-bandwidth limits in integrated lithium niobate modulators using micro-structured electrodes. *Optica*, 8(3):357–363, 2021.